Landslides
DOI 10.1007/s10346-017-0932-6
Received: 7 June 2017
Accepted: 3 December 2017

Danqing Song · Ailan Che · Renjie Zhu · Xiurun Ge

Dynamic response characteristics of a rock slope with discontinuous joints under the combined action of earthquakes and rapid water drawdown

Abstract In order to study the dynamic response characteristics of a rock slope with discontinuities under the combined action of earthquakes and rapid water drawdown, a large-scale shaking table test was performed on a rock slope with discontinuous joints. Wenchuan earthquake (WE) seismic records were performed to investigate the horizontal and vertical acceleration response and displacement response. In particular, three-dimensional optical measurement techniques was used to obtain the slope surface displacements. A comparison was made on the seismic response according to the analysis of PGD (peak ground displacement) and M_{PGA} (acceleration amplification coefficient) of the modeled slope. The results show that the experimental slope mainly underwent settlement and horizontal deformation when the WE records were applied in the z and x directions, respectively. The slope was first shaken by the P wave, which caused the differential settlement to occur at the surface slope; then, the slope was shaken more severely by the S wave, which led to a greater horizontal deformation. Moreover, analysis of the ΔPGD (increment of PGD) and ΔM_{PGA} (increment of M_{PGA}) under rapid drawdown suggests that the rapid water drawdown mainly impacts the deformation of the surface slope, particularly between the high and low water levels. The water infiltration through the cracks softened the material of the surface slope, and the rapid drawdown also enhanced the slope deformation. In addition, the damage evolution process of the slope can be identified, mainly including three stages: an elastic stage (< 0.168 g), a plastic stage (0.168–0.336 g), and a failure stage (> 0.336 g).

Keywords Dynamic response characteristics · Damage evolution process · Earthquake · Rapid water drawdown · Rock slope · Discontinuous joints

Introduction

Earthquake-induced rock landslides cause destructive damage and fatalities worldwide (Jiang et al. 2015; Massey et al. 2017), and so their dynamic stability should be analyzed accurately (Huang and Li 2009; Huang et al. 2013). The Ms 8.0 Wenchuan earthquake occurred in Wenchuan County, Sichuan Province, China, on 12 May 2008, at the eastern edge of Qinghai-Tibet Plateau (Wang et al. 2009; Fan et al. 2016). The earthquake triggered extensive landslides and collapses (Zhang et al. 2014; Gao et al. 2017), which are the main geological disasters during the earthquake, including 56,000 landslides and rock falls, which lead directly to approximately 20,000 deaths (Huang and Li 2009; Dai et al. 2011). Field surveys of geological disasters (Wang et al. 2009, 2011), observed the phenomenon of wave propagation influencing slope stability. In Hongbai Town, Shifang City, Sichuan Province, 185 landslides and 93 landslides occurred on the back and facing slope, respectively, in the valley that is nearly perpendicular to the seismic fault (Wang et al. 2011). The proportion of landslides at each location indicates that the wave propagation triggered more landslides on the back slope. Moreover, most of the landslides near the earthquake epicenter were subjected to strong lateral S wave forces and were characterized by "throw-like collapses" (Che et al. 2016). P and S waves have significant impact on the rock slope stability during earthquakes. Therefore, the dynamic stability of rock slopes has been one of the most important topics in geotechnical and seismic engineering (Garevski et al. 2013; Shinoda 2015).

The dynamic response characteristics of rock slopes with complex geological structure has been studied by many researchers, particularly rock slopes with discontinuous joints. Normally, the distribution of joints within a rock mass shows typical discontinuity, and the discontinuities play an important role in wave propagation (Che et al. 2016). Weak structural surfaces contain a large amount of discontinuous joints in rock masses, and the mechanical properties of rock masses are further deteriorated due to the extension and convergence of the joints. In particular, the geometric and mechanical parameters of discontinuous joints, especially the direction, angle, and location of the joints, have a substantial impact on the slope stability (Jiang et al. 2013). Therefore, the dynamic response of rock slopes with discontinuous joints under seismic excitation have been much more complicated due to the complex composition of geological materials and discontinuities in rock masses (Wang et al. 2009; Xu and Yan 2014; Dong et al. 2015; Che et al. 2016).

Reservoir water level fluctuation has been one of the most important causal factors in the slope failure of reservoir banks (Berilgen 2007; Xia et al. 2013; Lu et al. 2015; Maihemuti et al. 2016). The pore pressure and seepage pressure increase gradually as water infiltrates into the slope, and eventually lead to a change in the slope stability, in the process of water level fluctuation (Maihemuti et al. 2016). Water level fluctuation has an impact on the flow direction of the water between the rock slopes and the reservoir, which leads to the varying pore-water pressure levels in slopes. The rock mass structure is in a dynamic state, balancing the stress from both the bank rock pore-water pressures and the reservoir water level via deformation to generate space for the flow of water within the rock matrix (Huang et al. 2016). It has also been acknowledged that water drawdown is a key triggering factor of slope failure (Gao et al. 2014; Moregenstern 2015). In addition, western China is an earthquake-prone region, particularly the seismic belt distributed in the Yunnan-Kweichow Plateau. The stability of the reservoir bank landslides has become an urgent problem during construction of large-scale projects in western China. The stability of a reservoir bank slope can be complicated due to the combined influence of the reservoir water and earthquakes, and their stability directly affects the operation of the engineering projects in the area. Therefore, special attention

Published online: 19 December 2017

should be paid to the issue of rock slope stability under the combined influence of earthquakes and reservoir water level.

Great efforts have been made to analyze the slope failures induced by earthquakes using various approaches. Field observation, numerical calculation, and physical model tests are the main methods in researching the seismic response of rock slope (Liu et al. 2014b). Numerical methods have been widely used to simulate the actual failure mechanisms of landslides, such as the finite element method (FEM) (Toki et al. 2010), the discrete element method (DEM) (Jiang et al. 2015), the discontinuous deformation analysis (DDA) (Song et al. 2016), et al. In particular, numerical methods have been used for the dynamic analysis of rock slopes under seismic excitation; for example, to study the dynamic deformation process (Jiang et al. 2015) and wave propagation characteristics (Che et al. 2016) as well as analyze discontinuous deformation (Fu et al. 2016). However, using numerical methods to study the dynamic stability of slopes has a few disadvantages. For example, FEM dynamic analysis is not suitable for large deformation problems, discontinuous rock mass problems, infinite domain problems, and stress concentration problems. DEM is suitable for the discontinuous medium of large deformation problems but has limitations for continuous media. DDA is applicable in the simulation of the deformation process of blocks but has limitations for the selection of rock mass parameters. In particular, for complex rock mass slope structures, it is difficult to collect enough earthquake recordings by using the abovementioned methods due to the unpredictable occurrence of earthquakes, and these methods cannot accurately evaluate the seismic response due to the simplifications of the boundary conditions, mesh generation, and parameter selection. In recent years, shaking table tests have been used to simulate the variation of dynamic response of rock slopes and directly reveal the failure modes of structure under seismic excitation (Chen et al. 2016; Fan et al. 2016), allowing various types of lithology combinations and structures to be studied, in particular, slopes with discontinuous joints (Che et al. 2016) and slopes with weak intercalation (Chen et al. 2016; Fan et al. 2016). In large-scale shaking table tests, the model size, the ground motion input parameters, and waveforms can be controlled based on the case studies to enable the slope dynamic responses to be measured to greater accuracy (Hong et al. 2005; Lin and Wang 2006; Lin et al. 2015; Yang et al. 2012). Therefore, the shaking table test method has been one direct way to simulate the variation of dynamic response of slope and directly reveal the failure modes of structure under seismic excitation (Chen et al. 2016; Fan et al. 2016).

Many researchers have studied the dynamic acceleration response of a rock slope, which is regarded as a continuous medium, based on the analysis of acceleration (Lin and Wang 2006; Huang et al. 2013; Liu et al. 2014a; Fan et al. 2016). However, the analysis of acceleration is a qualitative analysis method for rock slopes with complex geological structures, and errors can arise if the acceleration sensors are damaged during the vibration, which may lead to the inaccurate assessment of the measured dynamic response. The analysis of surface displacement has been a direct, visible, and reliable method to reflect the dynamic deformation and failure of slopes. In particular, the displacement data acquisition is carried out by non-contact photographic technology, with no interference by seismic load. Moreover, the dynamic response of a rock slope that is modeled as a non-uniform continuous medium with discontinuous joints has not been widely discussed in terms of the surface displacement response; the analysis results are more reliable by using the simultaneous dynamic acceleration and surface displacements. These dynamic response characteristics also have not been widely studied with large-scale shaking table model tests; therefore, there is only a small amount of information on the analysis of the dynamic response of slopes due to earthquakes and rapid water drawdown.

This work takes an actual engineering project as an example, and a large-scale shaking table test was successfully performed on a slope with discontinuous bedding and counter-bedding joints under rapid water drawdown. Compared with previous studies, the geological structure of the model slope is very complicated in the test, and displacement measuring device is more accurate, in particular, the dynamic response characteristics of the slope was analyzed under the combined action of seismic excitation and rapid water drawdown. The analysis of the slope dynamic response characteristics has been derived from two aspects in this research-displacement response of the slope surface and acceleration responses of the slope. Accelerometers were installed in the slope to monitor the acceleration, and a high accuracy displacement measurement system, the extended three-dimensional digital image correlation (XTDIC) system that utilizes three-dimensional optical measurement techniques, was used to obtain the slope surface displacements. Moreover, the influence of wave propagation directions on the slope deformation is studied, and the failure mechanism of the landslide induced by the P waves and S waves was also analyzed by analyzing the PGD and M_{PGA}. The influence of rapid water drawdown on the slope deformation is also clarified by using ΔPGD and ΔM_{PGA}. In addition, the failure mode of the slope composed of blocks and its evolution process of the damage due to deformation is identified under the combined action of earthquake excitation and rapid water drawdown, according to the analysis of the PGD and M_{PGA}. This work also discusses which method is more suitable for the analysis of the slope deformation characteristics, given the comparative analysis of the PGD (ΔPGD) and M_{PGA} (ΔM_{PGA}).

Shaking table tests

Case study

The proposed extra-large bridge of the Xiangli Highway over the Jinsha River is in the transition zone between the southeast edge of the Tibetan Plateau and the Yunnan-Kweichow Plateau in Southwest China (Fig. 1). The Lijiang River bank slope is located on the right bank of the Jinsha River, and the average natural gradient of the slope is approximately 40° (Fig. 2). The gradient of the pier is approximately 30°. The soil thickness on the slope surface is 0–5 m, including the colluvial slope rock soil and brecciated soil. Many toppling joints and three bedding weak structural planes developed in the rock mass, and the mountain unloading effect is strong. The distance between toppling joints is approximately 70 m, and the distance between bedding structural planes is approximately 35 m. The geomorphology of the Lijiang slope is shown in Fig. 2b. Direct shear tests were performed to obtain the cohesive force (c) and internal friction angle (ϕ). Uniaxial compression tests were performed to obtain the elasticity modulus (E) and Poisson's ratio (μ). The material parameters of the slope mass and weak intercalated layers are shown in Table 1. The proposed

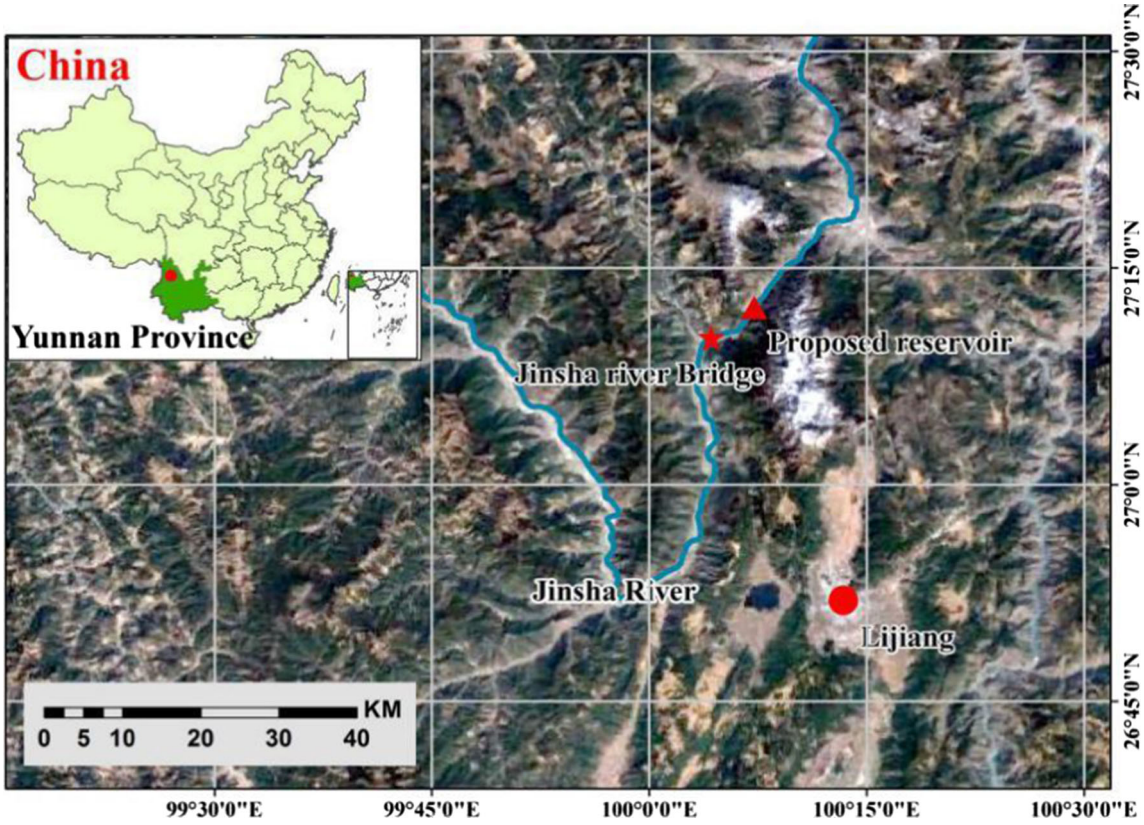

Fig. 1 Location of the study area on the Xiangli highway

bridge is located in earthquake-prone region, and a proposed reservoir will be built in the upper reaches of the bridge. Earthquake and rapid water drawdown may be the main triggers of the reservoir bank landslides, particularly, under the combined influence of their combination.

Technical background

A large-scale shaking table test was performed to elucidate the dynamic response characteristics and failure mode of a rock slope with discontinuous joints, under the combined action of the reservoir water and earthquakes. Acceleration sensors were used to record the acceleration-time curve and to clarify the dynamic acceleration response. The XTDIC measurement system was adopted to analyze its dynamic surface displacement response. An additional 10-cm-thick buffer layer was mounted on the base of the model to minimize the bottom boundary effect, where the materials of the buffer layer are similar to that of the slope. To eliminate the adverse effects of the wave propagation, a wave

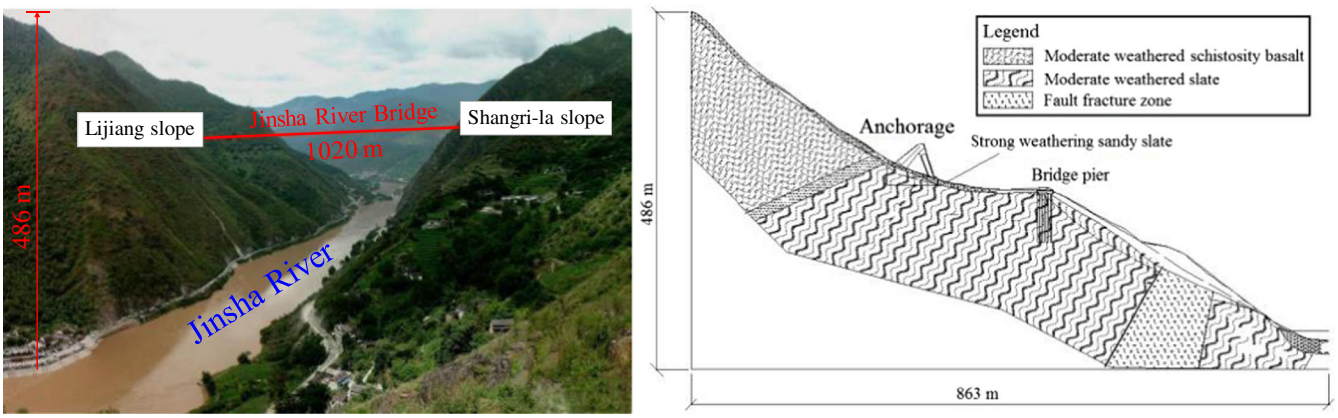

Fig. 2 **a** Topography and geomorphology of Lijiang slope and **b** geological section of Lijiang slope

Table 1 Physico-mechanical parameters of material parameters of the slope

Physico-mechanical parameters	Density ρ/kN/m^3	Poisson ratio μ	Dynamic elastic modulus E/GPa	Friction angle ϕ (°)	Cohesive force c (MPa)
Rock mass	28.5	0.30	10.0	49.0	1.92
Structural surface	28.5	0.35	10.9	36.1	2.30

absorber was installed. The wave absorber consisted of a porous sponge stuffing and iron gauze, which was placed in the end of the model box, as shown in Fig. 3b. Many details are considered in the test, which ensured that its analytical results are reliable and accurate. The materials and test parameters of the model slope were obtained based on the Buckingham π theorem of similarity.

Shaking table

A bi-directional (horizontal and vertical) electric servo shaking table was used in the tests. The shaking table was made by Japan Kokusai Corporation, and the tests were performed in the Key Laboratory of Loess Earthquake Engineering, Gansu Earthquake Administration. The shaking table is 4 m wide and 6 m long (4 m × 6 m) and utilizes a single, horizontal translation degree of freedom. The maximum load of the shaking table is 25 t, with its maximum horizontal and vertical accelerations being 1.7 and 1.2 g, respectively. The effective frequency range of input motion is 0.1 to 70 Hz, with regular and irregular waves can be used as input motions.

Experiment tank and scaled model

An experimental tank was developed for the tests, in which the inside of the box is 2.8 m × 1.4 m × 1.4 m. It was designed as a rigid, sealed box with carbon steel plates and organic glass, as shown in Fig. 3a. Because the proposed anchorage and pier are all located in the sandy slate (Fig. 2b), the similar material of slate was used to simulate the rock mass in the model slope, rather than basalt. The model slope is simplified based on the geological section of Lijiang slope (Fig. 4). The pouring process of the large volume model, differing casting times, could cause some issues, such as differing material characteristics. The slope model was constructed with prefabricated blocks, which were piled up in four layers. The volume and packing way of the prefabricated blocks were determined based on the design dimensions of the model slope, as shown in Fig. 3. The production process of individual modules is shown in Fig. 5. Rectangular templates are used as blocks templates, as shown in Fig. 5a. For the bottom and surface slope, blocks were cut to make non-rectangular blocks, as shown in Fig. 5d. Discontinuities were simulated by gray paperboard, which was glued to the surface of the blocks between the two layers, as shown in Fig. 5. Based on the Buckingham π theorem of similarity, the average thickness of discontinuous joints in the model slope is < 2 mm, indicating that its thickness and cohesive force can be ignored, but its internal friction angle should be simulated accurately. Gray paperboard also owns a few advantages: larger thickness and density, longer fiber, good toughness, bigger strength, and better water stability. Direct shear experiments showed that the internal friction angle of gray paperboard are the most similar to that of discontinuous joints. The materials in the model slope were mainly formed of barite, steel slag, sand, plaster, and water at ratios of 5:4:1.3:2.1, according to a series of triaxial tests. The bottom surface of the model slope was 186 × 140 cm in size and 89 cm in elevation. The angles structural plane and discontinuous reverse joints slope were set 15° and 75°, respectively, in the model material, as shown in Fig. 4. The parameters of the rock masses were found to be a friction angle of $\phi = 49°$, cohesion of $c =$ 0.048 MPa, shear modulus of $G_o = 25$ MPa, density of $\rho = 28.5$ (kN/m^3), and Poisson ratio of $\mu = 0.30$.

Measurements

The measurement points of acceleration sensors are shown in Fig. 6. Firstly, 20 accelerometers were installed in the slope. A three-direction capacitive acceleration sensor (DH301) was used in the test, which is made by Donghua Testing Co., LTD. The frequency range of acceleration sensor is 0–1500 Hz in horizontal and 0–800 Hz in vertical, and its sensitivity is about 66 mV/m s^{-2}

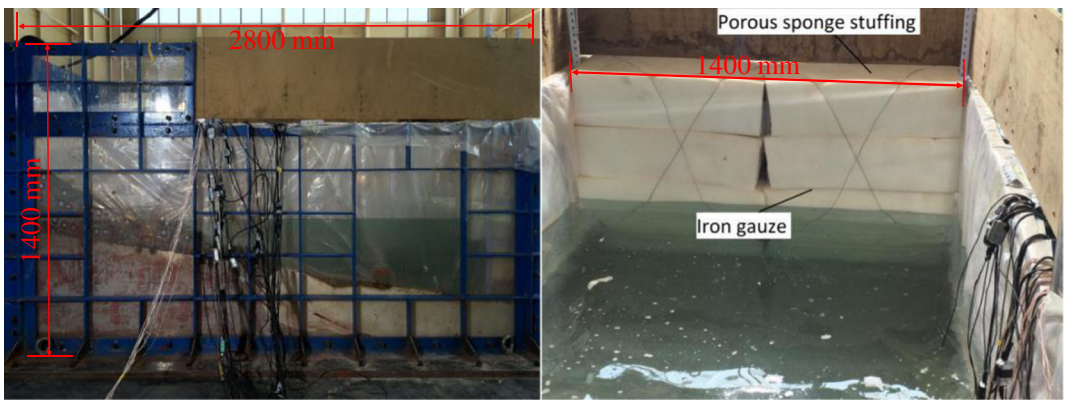

Fig. 3 **a** Soil container and scaled model and **b** wave absorber in the soil container

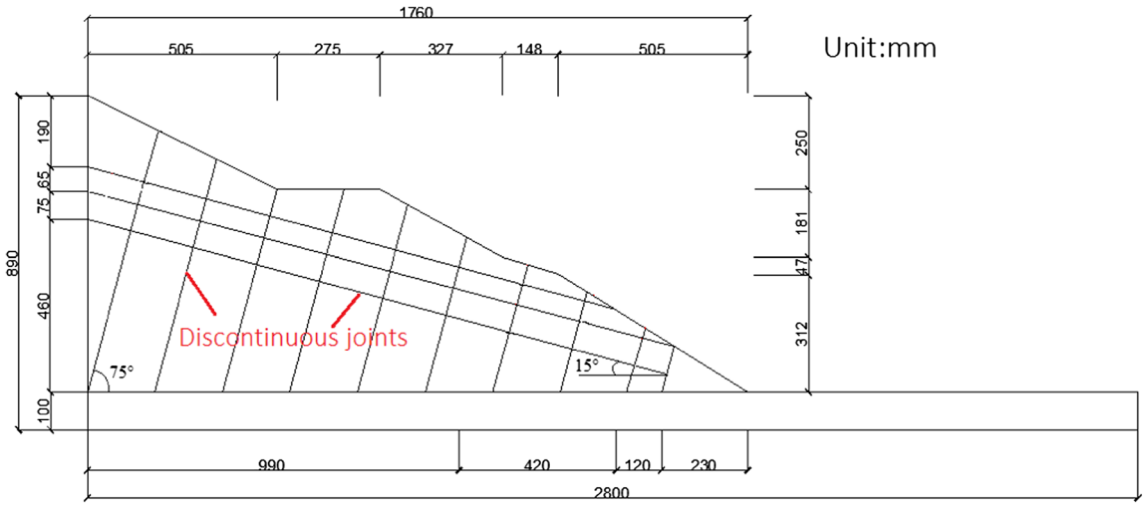

Fig. 4 The model slope profile

with the measuring range (Peak) being ± 20 m/s². All of the acceleration sensors were embedded into the center of the slope model, in order to reduce the side boundary effect. Additionally, to track the displacement of the slope subjected to seismic loads, an optical measurement technique was also employed. The displacement data were collected by using the XTDIC measurement system. This system includes two cameras that each have a resolution of two million pixels, and it has an acquisition frequency of 50 Hz, as shown in Fig. 7. One camera was used to collect the displacement data of the surface slope in the *y* and *z* directions, and the other camera was used to collect the displacement data in the *x* and *z* directions. The highest acquisition frequency of the XTDIC measurement system is 340 Hz, and its measurement error is approximately 0.05–0.1 mm, within a range of 5 m from the experimental slope. The deformation was observation on slope surface, and 14-mm non-coding marker points were used at an initial separation distance of 100–150 mm. The three-dimensional displacement of every marked point was obtained in the tests, and the layout scheme of the marked points is shown in Fig. 8.

The XTDIC measurement system is based on binocular stereo vision technology, and it uses two high-speed cameras to collect the real-time images in all stages of object deformation. The accurate recognition of the marker points or digital speckle can be used to achieve stereo matching, including the coding and non-coding marker points, which were used to reconstruct the three-dimensional coordinates and displacements of the surface points and to calculate the deformation of the object. This method is highly precise, is fast and easy to operate, and does not involve

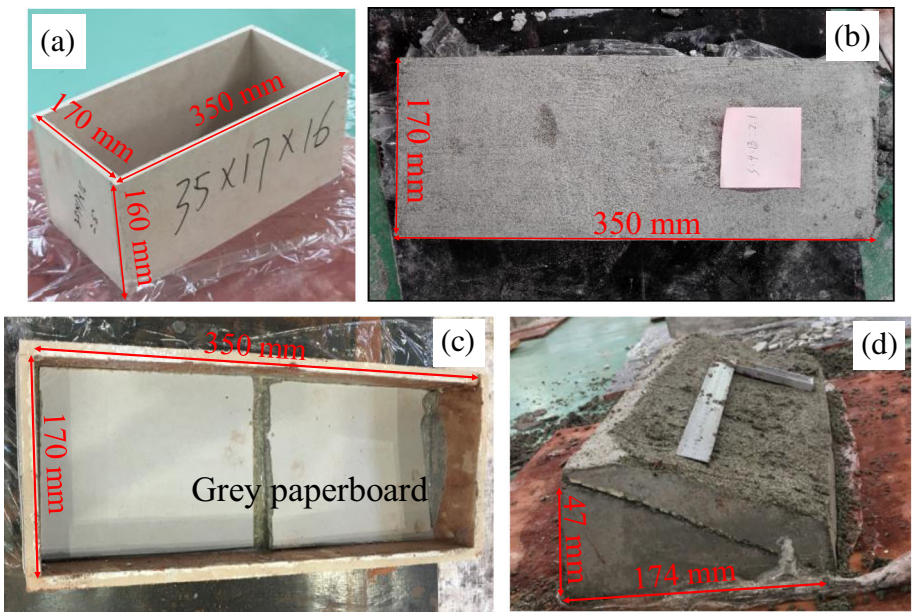

Fig. 5 Prefabricated blocks production. **a** Block mold, **b** prefabricated blocks, **c** Gray paperboard, and **d** non-rectangular blocks production

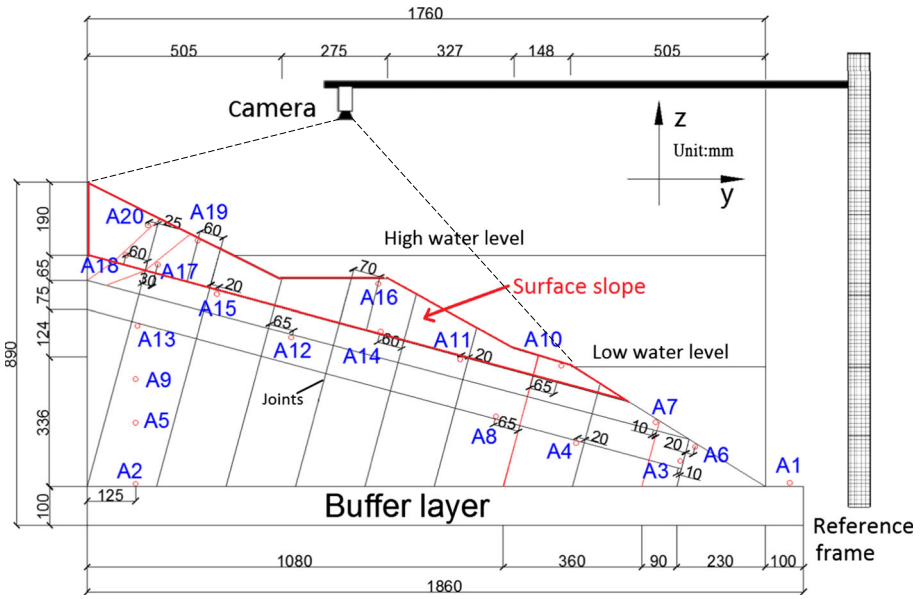

Fig. 6 Layout of measurement points and accelerometers

contact. Figure 9 illustrates the displacement vector tracking process and measuring principle. The cameras were stationary after calibration and collected a few images when the model is static, as a benchmark. When the shaking table began to shake, the cameras began to collect the displacement data. Finally, the spatial coordinates of each of the marker points are calculated in each image, and the displacements of the marker points can then be obtained. In brief, the displacement data were obtained according to the analysis of the change in coordinates. The data analysis of the XTDIC measurement system supports coordinate transformation. If the built-in coordinate system of the XTDIC cannot meet the requirements of the experiment, exact coordinates should be acquired by using the 321 conversion mode built into the system.

Input motions

The seismic wave was simulated by inputting acceleration-time history curve in the process of shaking table tests. The time history and the Fourier spectrum of wave are shown in Fig. 10. The vertical and horizontal Wenchuan earthquake records recorded by Wudu in Gansu of China are shown in Fig. 10. The dominant frequency of WE wave is 7.74 Hz. Two simultaneous loading directions of experimental earthquake excitation (the z and x directions) were applied in the tests. The working conditions of the tests are shown in Table 2. The purpose of setting high and low water levels during the test is to analyze the influence of the water drawdown on the dynamic characteristics of the slope. However, due to the waterproofing measures, the water cannot be quickly released, and the rapid drawdown was only modeled by rapidly drawing water out of the experiment tank. Moreover, the water cannot be drawn out of the experiment tank successfully during the process of vibration, because the vibration time is very short. Given these restrictive factors, the rapid drawdown was modeled by drawing water out rapidly, when the shaking table vibrations were not applied. Therefore, the rapid water drawdown during the test is used to analyze its unloading effect on the slope body.

The acceleration data from the test requires reprocessing, primarily by filter and baseline calibration, as the collected acceleration-time curve includes both systematic error and human

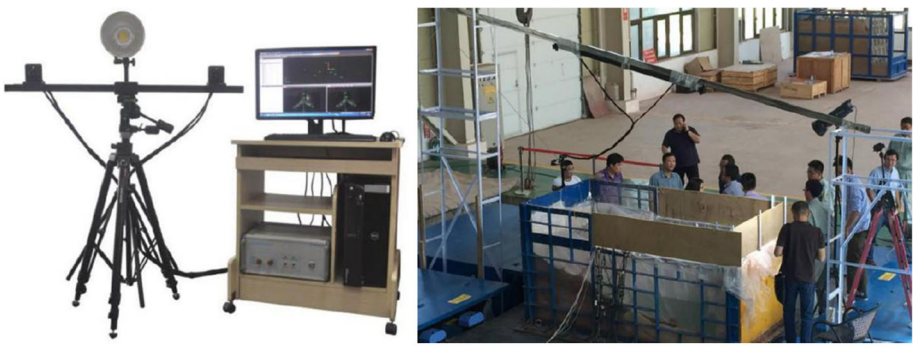

Fig. 7 **a** XTDIC optical measurement system and **b** layout position of XTDIC optical measurement system

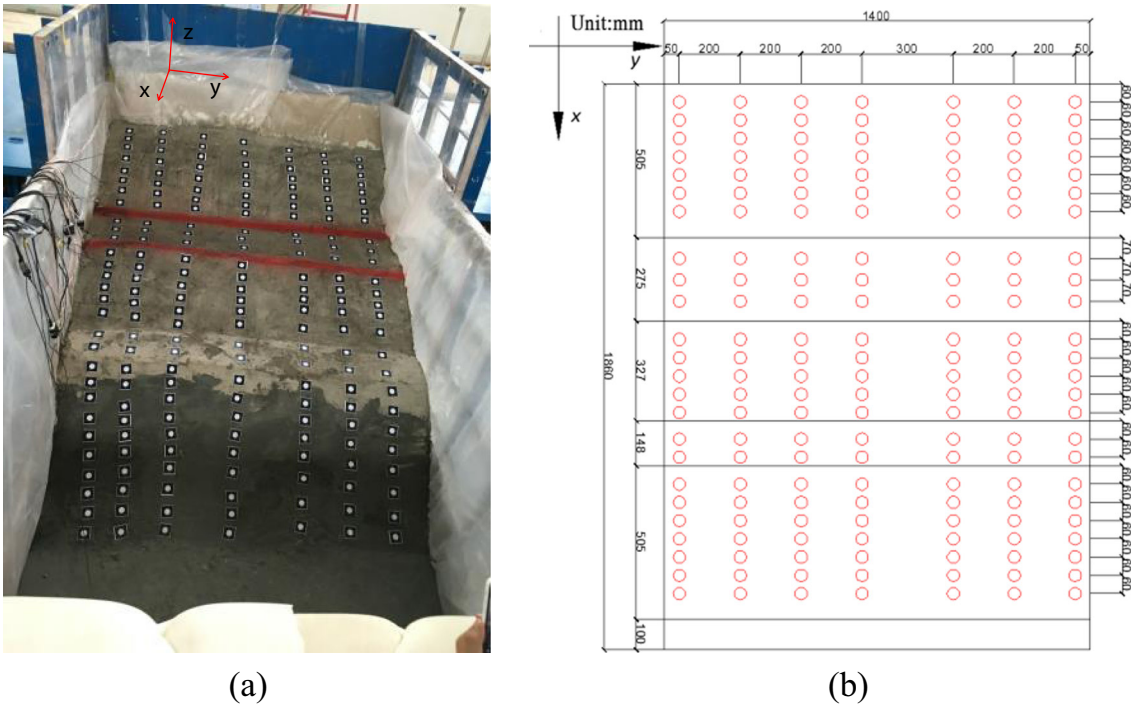

Fig. 8 Layout of mark points of surface displacement. **a** Model slope and **b** sketch map

error. First, the effective waveform frequency was mainly in the range of 3~50 Hz, since the acquisition waveforms contained many high-frequency waves. MATLAB was used to compile the Chebyshev II bandpass filter, which was used to filter the wave, and it can attenuate quickly without allowing the passband to fluctuate. Second, the initial value of the response waveform will drift because of the vibration, and the baseline drift data should be subtracted out of the initial value in the waveform processing.

Dynamic response of the slope during an earthquake

Dynamic displacement response

In the tests, the slope surface mainly displaced in the x and z directions, when the input seismic wave was created in a certain direction. It was observed that the main slope displacements were in the same direction as the input wave. This observation indicates that the main settlement deformation and the main sliding deformation were induced by the P wave and S wave, respectively. It also indicates that the wave propagation direction has a dominant effect on the displacement of the surface slope. Therefore, the horizontal and vertical displacements of the slope surface, when the seismic wave was input in the x and z directions, respectively, were used to analyze the dynamic response characteristics of the slope. The vertical and horizontal PGD of the slope surface are shown in Fig. 11. The PGD is not obtained at 0.504 g, since the marker points had fallen off of the slope surface. In addition, the PGD is only obtained above the water level, because the high-speed cameras were unable to collect the images of marker points underwater.

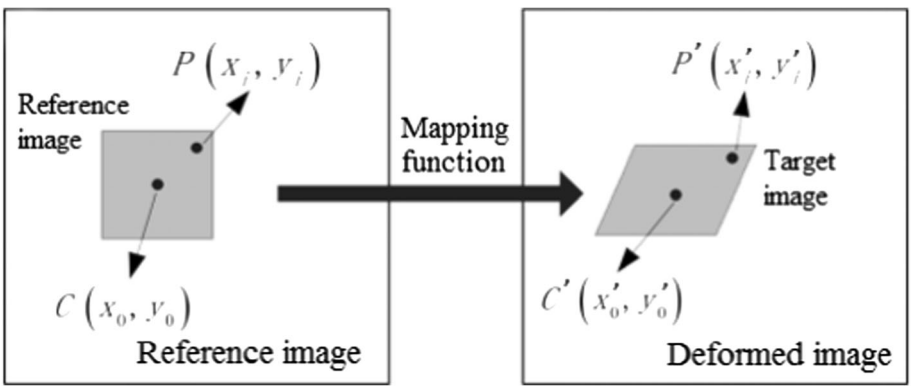

Fig. 9 Illustration of displacement vector tracking process

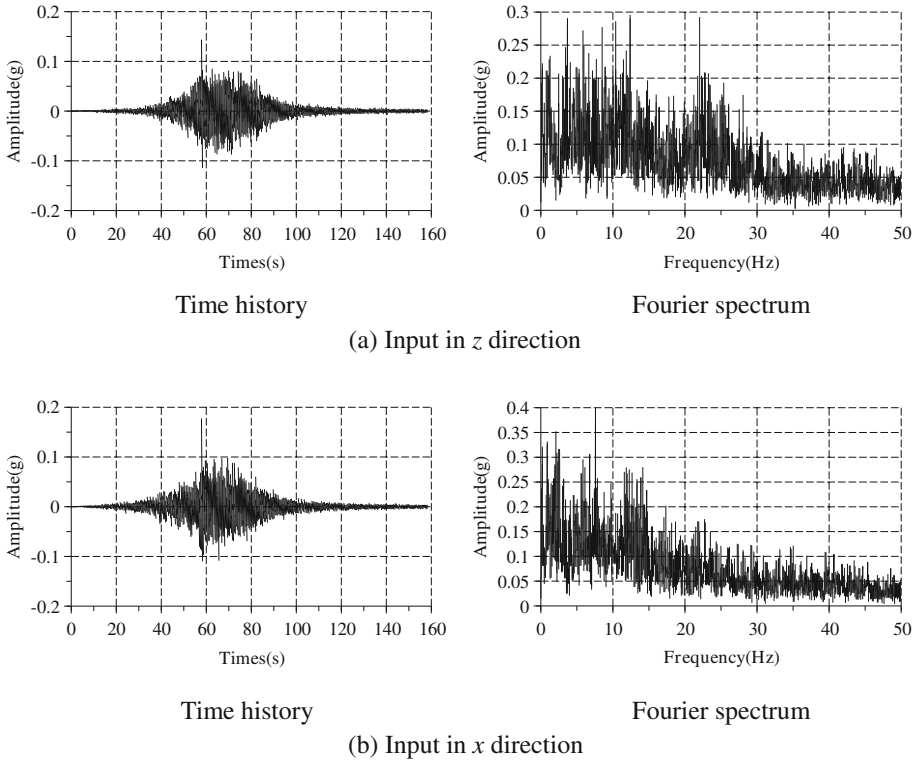

Fig. 10 The input WE records showing **a** input in z direction and **b** input in x direction

The wave propagation direction has a great effect on the dynamic response of the slope. Figure 11 shows that the settlement is the main deformation when the input is in the z direction and that horizontal sliding is the main deformation when the input is in the x direction. In addition, the PGD measured when the input wave is in the x direction (PGD_x) is much larger than that when the input is in the z direction (PGD_z). The PGD_x is approximately 1.3–1.5 times as large as the PGD_z. Therefore, the horizontal deformation is the primary deformation, and the S wave has a greater impact on the deformation of the slope. In addition, Fig. 11 shows that the PGD increases with the increasing earthquake intensity. When the earthquake intensity is < 0.168 g, the PGD is small, and the slope is stable. When the earthquake intensity is 0.336 g, the PGD increases rapidly, indicating that a large deformation appears in the surface slope. Additionally, Fig. 11 shows that the S wave has a great influence on the surface displacement of the platform and that the PGD is larger than that of the adjacent area, since the slope gradient substantially changes near the platform. However, the PGD of the platform is smaller and close to the adjacent area, indicating that the P wave has little influence on the displacement in the area.

The differential deformation between adjacent blocks is the main triggering factor of the rock landslide under seismic loading. Figure 11a shows the PGD_{max} and PGD_{min} are approximately 7.1 and 3.5 mm, respectively, when the seismic intensity is 0.084 g and the seismic load is vertical. It can also be found that the PGD_{max} and PGD_{min} are approximately 4 and 9.75 mm, respectively, when the seismic intensity is 0.168 g. However, when the seismic intensity is 0.336 g, the PGD_{max} and PGD_{min} are 21.5 and 10 mm, respectively. It can be found that the difference between the PGD_{max} and PGD_{min} are 3.6, 5.75, and 11.5 mm when the seismic intensity is 0.084, 0.168, and 0.336 g, respectively. These results indicate that when the seismic intensity is < 0.168 g, the settlement difference of the surface slope is small, and the slope is stable. In this stage, the longitudinal tensile deformation occurs and a few cracks appear because of the differential settlement between the blocks in the surface slope. However, the difference

Table 2 The test loading sequence

Amplitude (g)	0.084	0.084	0.168	0.168	0.336	0.336	0.504	0.504
Water level	High	Low	High	Low	High	Low	High	Low
No.	1	2	5	6	9	10	13	14
Vibration direction	z	z	z	z	z	z	z	z
No.	3	4	7	8	11	12	15	16
Vibration direction	x	x	x	x	x	x	x	x

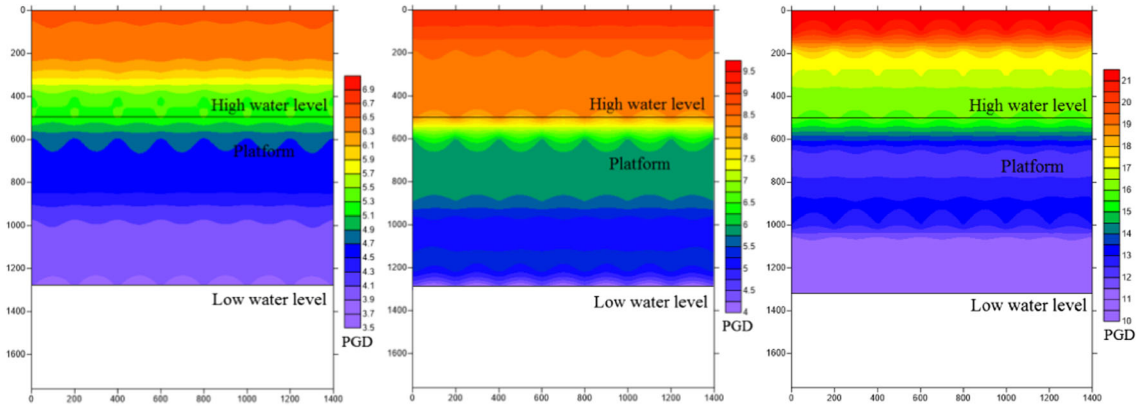

Acc.$_{max}$=0.084g Acc.$_{max}$=0.168g Acc.$_{max}$=0.336 g

(a) Input in z-direction

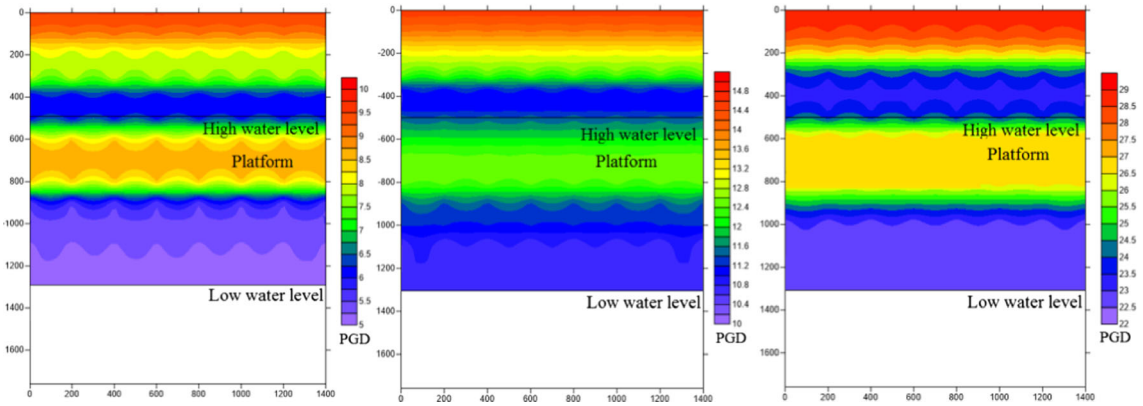

Acc.$_{max}$=0.084g Acc.$_{max}$=0.168g Acc.$_{max}$=0.336 g

(b) Input in x-direction

Fig. 11 Distribution of PGD when input WE wave under low water level for **a** in z direction and **b** in x direction

between the PGD_{max} and PGD_{min} rapidly increases when the seismic intensity is 0.336 g. Many penetrating cracks also appear, and the surface slope produces a large deformation and began to fail due to large settlement difference between the blocks. In addition, the settlement difference between the PGD_{max} and PGD_{min} increases with increasing earthquake intensity, indicating that the deformation of the surface slope also increases. The surface slope changes are similar when the seismic input is in the x direction and z direction, as shown in Fig. 11b. In these cases, uneven horizontal slide appears between the blocks; in particular, the PGD of the front block is larger than that of the back block, which leads to tensile fracture formation between the blocks. Given the analysis of the differential deformation, the differential deformation between the adjacent blocks directly leads to the occurrence of landslides under seismic excitation.

Therefore, the deformation of rock slopes is induced by P and S waves. First, the P waves shook the slope vertically and lateral cracks were induced on the slope surface, and the settlement deformation was observed, which weakens the rock slope stability. Second, a larger horizontal shear deformation of the rock slope was induced by the strong horizontal shaking from the S-waves, which led to the sliding deformation of the surface slope. Most of the landslides near the epicenter of the Wenchuan earthquake were also subjected to strong lateral S wave forces and characterized by "throw-like collapses" (Che et al. 2016); the larger horizontal earthquake throwing force was closely related to the amplification of the horizontal seismic acceleration.

Dynamic acceleration response

PGA (peak ground acceleration) is the peak value of acceleration at each measuring point, and M_{PGA} is the ratio of the PGA and peak acceleration of the shaking table surface. The M_{PGA} distribution is shown in Fig. 12, and the M_{PGAmax} of the slope is shown in Table 3. Wave propagation directions have a great influence on the acceleration response of the slope. Figure 12 shows that the M_{PGA} due to a seismic input in the x direction (M_{PGAx}) was larger than that of a seismic input in the z direction (M_{PGAz}). On average, the $M_{PGAxmax}$ is approximately 1.2–1.3 times greater than the $M_{PGAzmax}$, as shown in Table 3. In addition, Fig. 12 shows that the magnified area of the surface slope during a horizontal earthquake loading is also larger than that during a vertical earthquake

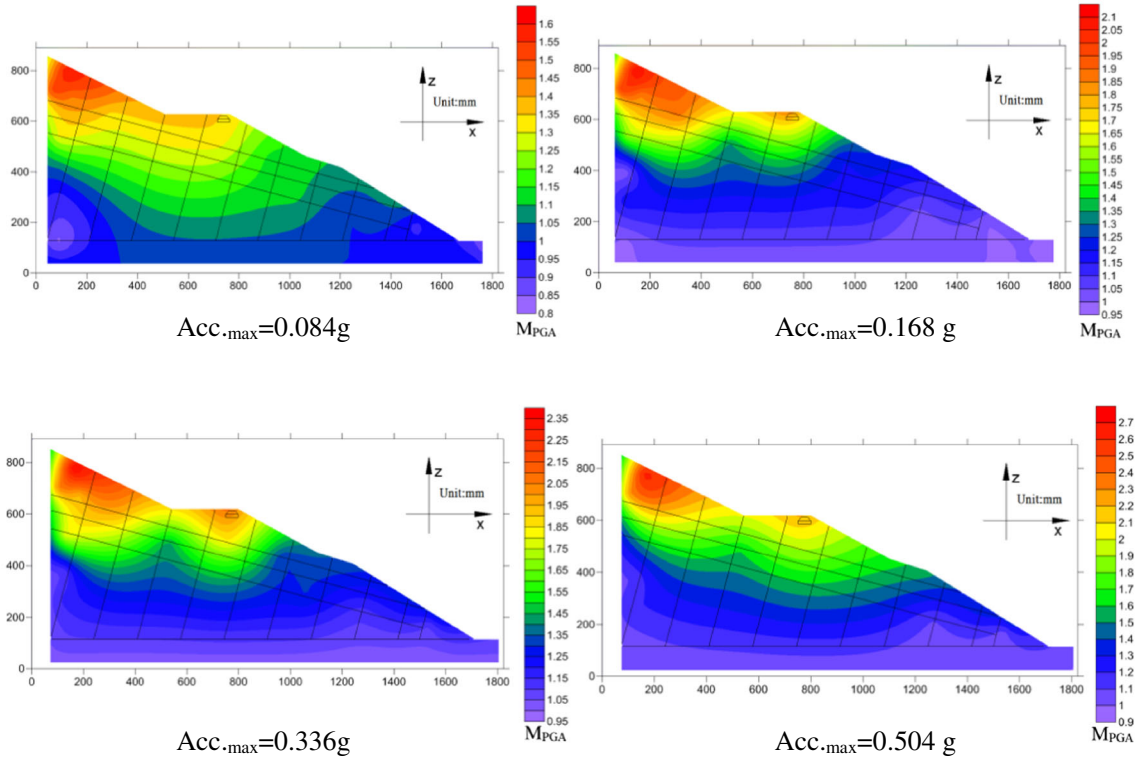

(a) Input in z-direction

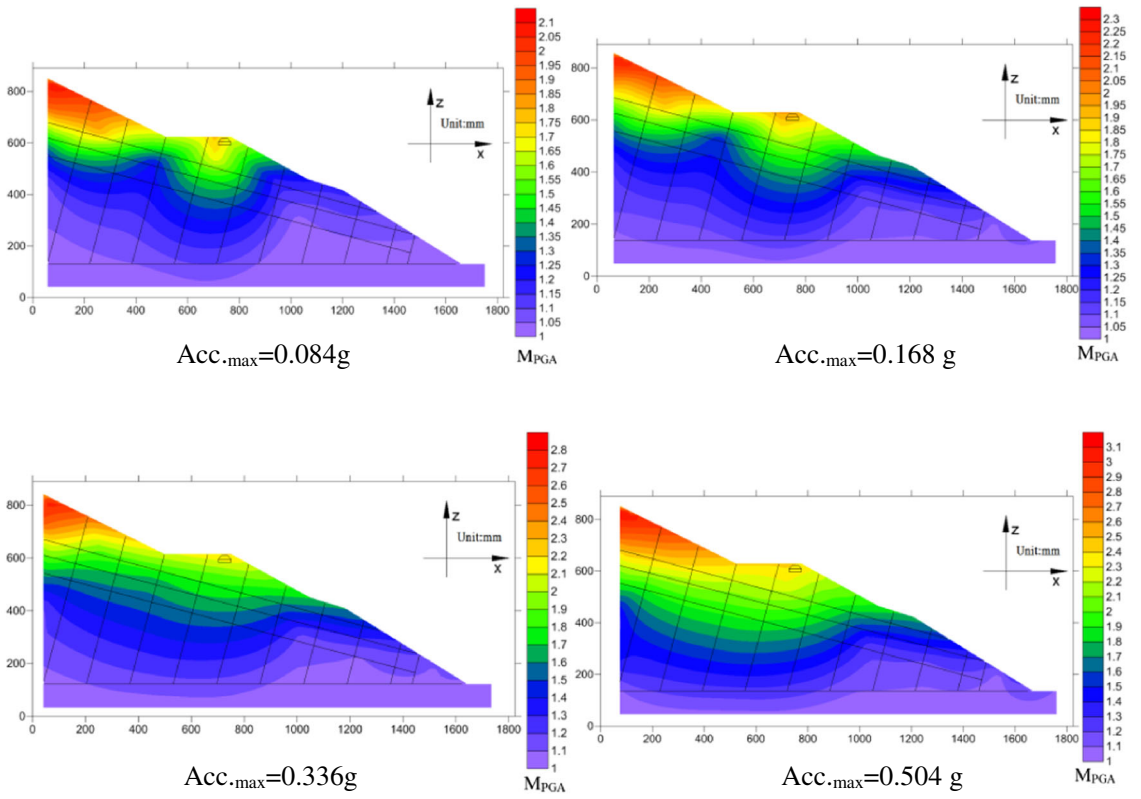

(b) Input in x-direction

Fig. 12 Distribution of M_{PGA} when input WE wave under high water level for **a** in z direction and **b** in x direction

Table 3 The M_{PGAmax} of the slope when input in x and z directions

Earthquake intensity (g)	0.084	0.168	0.336	0.504
$M_{PGAxmax}$	2.1	2.3	2.9	3.2
$M_{PGAzmax}$	1.6	2.1	2.4	2.8

loading. This is because the slope weight has an adverse effect on the amplification of the vertical acceleration, which leads to a restrained acceleration amplification effect in the z direction. During the earthquake, the slope deformation was mainly induced by the P and S waves. The slope was first shaken by the P wave. Differential settlement occurred in the surface slope, which led to the formation of many vertical cracks between the discontinuous joints and consequently the formation of the blocks, which ultimately increased the free surface of the surface slope. Then, the slope was shaken by S wave, and the inertial force of the surface slope becomes larger than that during the P wave shaking, which leads to a more marked magnification of acceleration than that created by P wave. Therefore, the magnified acceleration effect of the slope was more substantial when the seismic wave was input in the x direction, indicating that the slope deformation was triggered by the S wave.

Evolution process of damage deformation

Three blocks between the experimental high and low water levels were selected as examples to clarify the evolution process of deformation and failure of the slope, and the PGD and M_{PGA} of the surface slope are analyzed in Fig. 13. The three blocks include block 1 (A10), block 2 (A11), and block 3 (A16) from the low water level experiments, and the average PGD of the three blocks was used in this analysis. Figure 13 shows the evolution process of the damage deformation of the slope can be divided into three stages: stage 1 (< 0.168 g), stage 2 (0.168–0.336 g), and stage 3 (> 0.336 g). It should be noted that the PGD of the three blocks in stage 3 are predicted values. Due to the marker points falling off the slope surface in stage 3, the predicted values are based on two aspects. First, the increasing rate of the PGD clearly increases with increasing seismic intensity, and the PGD predictive values can be determined from the seismic intensity, within a certain range. Second, the lateral displacements can be obtained during the test, but they cannot be used to analyze the actual dynamic response because the lateral displacements were constrained by the model box walls, and their values were slightly smaller than that of the slope surface. However, the increasing trend between the lateral displacements and surface displacements is similar. Therefore, the PGD predictive values in stage 3 can be obtained within a certain range.

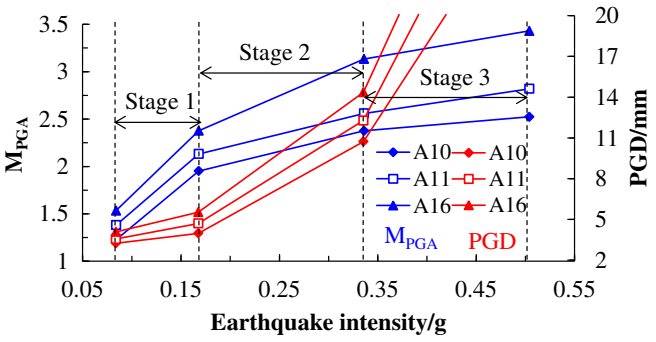

(a) Input in z-direction

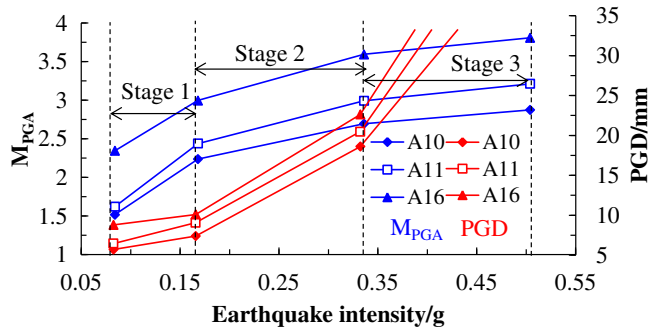

(b) Input in x-direction

Fig. 13 Relationship between M_{PGA} and PGD under low water level for **a** in z direction and **b** in x direction

Both the M_{PGA} and the PGD increase with the increasing earthquake intensity, but they increase at different rates. The rate of increase in the M_{PGA} decreases gradually with increasing earthquake intensity, while the rate of increase in the PGD continuously increases. First, the M_{PGA} increases rapidly in stage 1 because no clear deformation occurs in the slope. In stage 1, the PGD increases slowly, and the inertial force of the surface slope increases with increasing earthquake intensity, which leads to the rapid acceleration amplification effect. Second, the rate of increase in the PGD quickly increases in stage 2, while that of the M_{PGA} decreases to a certain degree. This is due first to the many cracks forming in the surface slope; as the experiment progresses, these cracks propagate, deepen, and often connect with the increase in the seismic intensity. It is notable that a large deformation occurs in stage 2 with much larger displacements, which makes the rate of increase in the slope inertial force decrease to a certain extent, which leads to an increased change in the decreasing amplification effect. Finally, in stage 3, the predictive PGD also quickly increases, and the M_{PGA} is generally stable, which indicates that failure begins; sliding along the slip surface occurs when the earthquake intensity reaches a certain value.

Therefore, the damage deformation process of the slope can be divided into three stages: elastic stage (< 0.168 g), plastic stage (0.168–0.336 g), and failure stage (> 0.336 g). Moreover, the damage deformation process of the slope can be identified by either the M_{PGA} or PGD. It is notable that a rapid increase in the PGD can be identified between damage stages. However, the change in the M_{PGA} is smaller, particularly in stages 2 and 3. This indicates that the damage deformation process of the slope can be elucidated by using the PGD, particularly if a large deformation of the slope occurs, and the rapid increase in the PGD can reflect the deformation more clearly than the M_{PGA}.

Dynamic deformation characteristic under the combined action of earthquakes and rapid drawdown

Earthquakes and rapid water drawdown are the two main triggers of reservoir bank landslides. The dynamic surface displacements and acceleration amplification effect were used

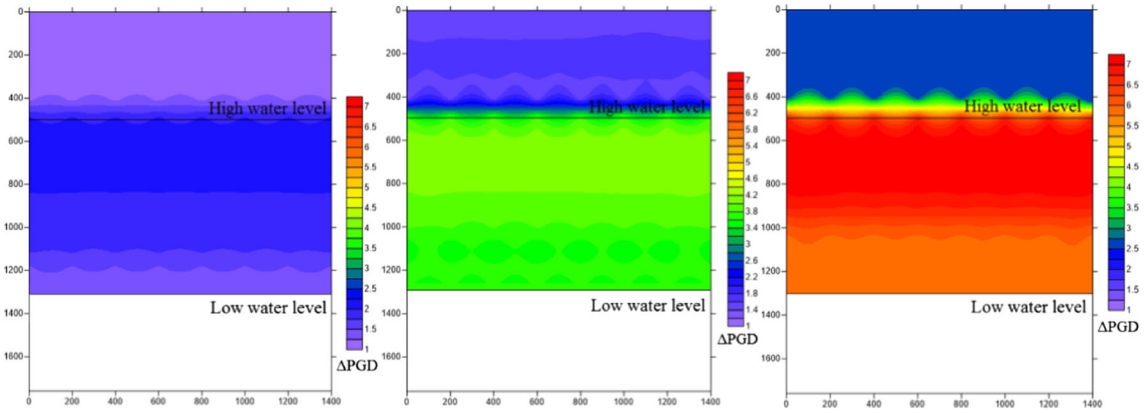

Acc.$_{max}$=0.084 g Acc.$_{max}$=0.168 g Acc.$_{max}$=0.336 g

(a) Input in z-direction

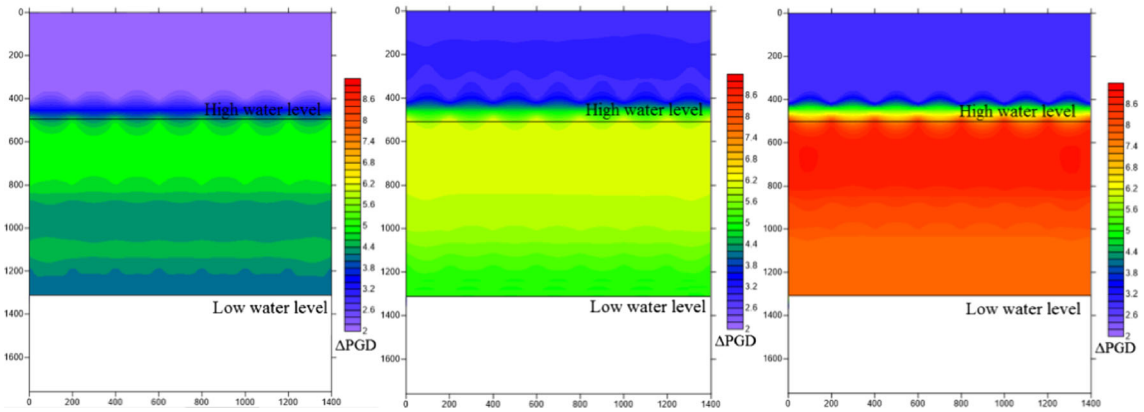

Acc.$_{max}$=0.084 g Acc.$_{max}$=0.168 g Acc.$_{max}$=0.336 g

(b) Input in x-direction

Fig. 14 Distribution of ΔPGD under rapid water drawdown for **a** in z direction and **b** in x direction

to analyze the influence of these two triggers on the dynamic deformation characteristics of the slope, by using the ΔPGD and ΔM_{PGA}.

Surface displacement

The distribution of the ΔPGD after rapid drawdown under seismic excitation is shown in Fig. 14, which shows that the PGD increases to a certain degree after rapid water drawdown under seismic excitation. It is notable that the ΔPGD between the high and low water levels is the greatest. This indicates that the rapid water drawdown has a greater impact on the surface slope deformation between the high and low water levels. The ΔPGD under the horizontal seismic loading is greater than that under the vertical seismic loading, indicating that the S wave has a greater impact on the slope deformation under rapid drawdown. In addition, Fig. 14 also shows that the ΔPGD increases with increasing earthquake intensity, particularly between the high and low water levels. For example, the ΔPGD_{max} are approximately 3, 4.7, and 7 mm when the input wave is in the z direction at 0.084, 0.168, and 0.336 g, respectively. Therefore, a more intense slope deformation is observed under the combined action of seismic excitation and rapid drawdown than under seismic excitation alone.

Acceleration amplification effect

The distribution of the ΔM_{PGA} after rapid drawdown under seismic excitation is shown in Fig. 15, which shows that the acceleration amplification effect of the slope increases after rapid drawdown. The ΔM_{PGA} of the surface slope is much larger than that of the internal slope, indicating that the rapid water drawdown has a greater effect on the surface slope than the seismic excitation. Moreover, Fig. 15 also shows that the ΔM_{PGA} between the high and low levels is the largest, indicating that the amplification effect between the high and low water levels is the most substantial during rapid water drawdown. Additionally, the ΔM_{PGA} of the surface slope under horizontal seismic loading is larger than that under vertical seismic loading. Therefore, the rapid drawdown has a great impact on the slope surface, particularly between the high and low water levels, and the amplification effect is more clearly affected by the S wave.

Additionally, Fig. 15 shows that the ΔM_{PGA} increases rapidly from 0.084 to 0.168 g between the high and low water levels and

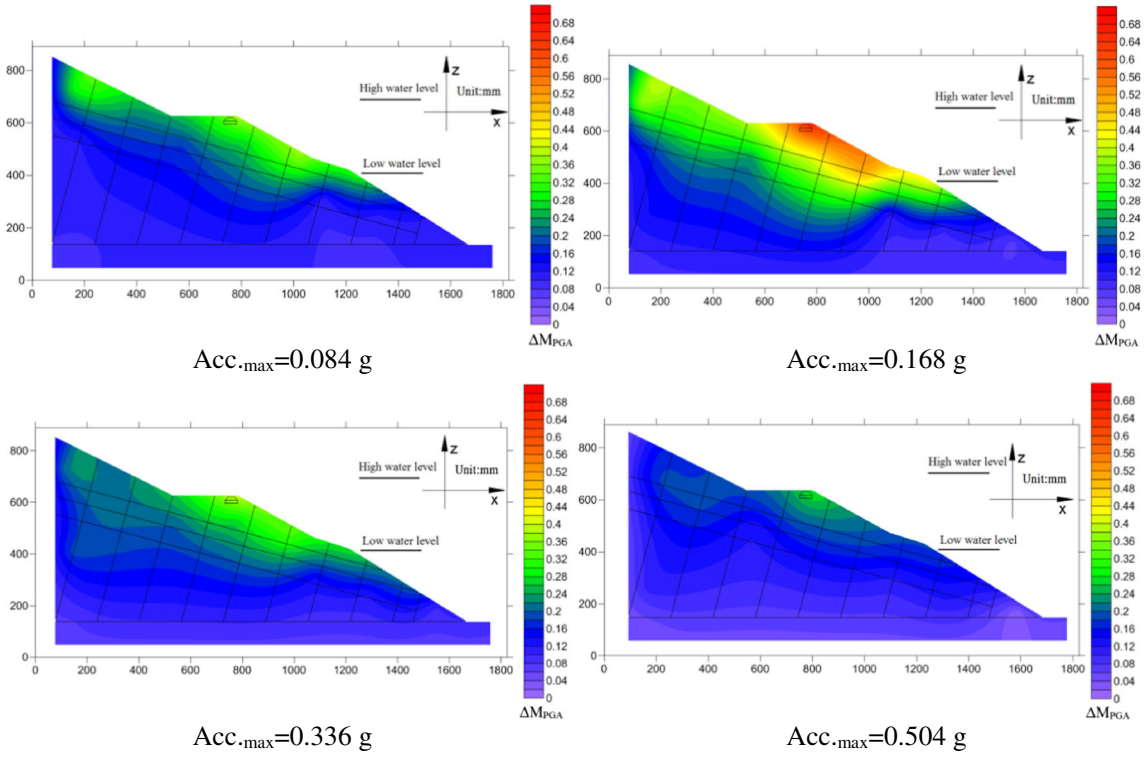

(a) Input in *z*-direction

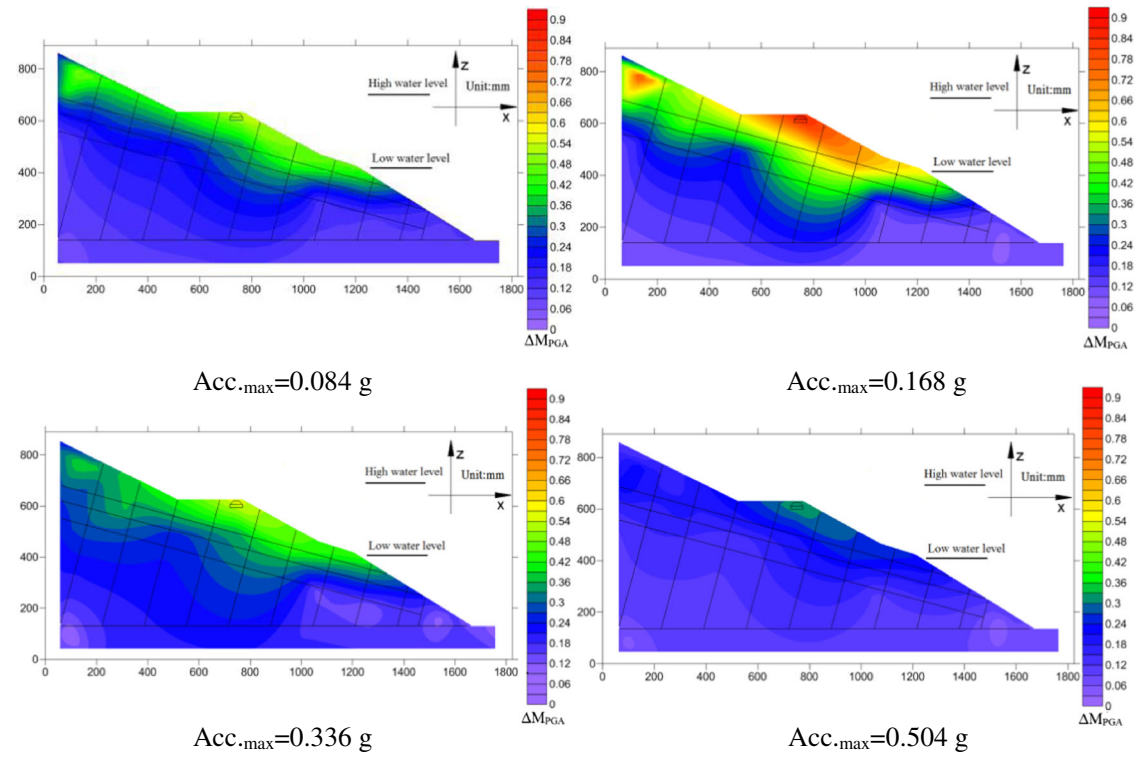

(b) Input in *x*-direction

Fig. 15 Distribution of ΔM_{PGA} after rapid water drawdown for **a** in *z* direction and **b** in *x* direction

then it decreases from 0.168 to 0.336 g, while the ΔM_{PGA} area remains fairly consistent. This observation indicates that the slope is stable when the ΔM_{PGA} is < 0.336 g. However, the ΔM_{PGA} later rapidly decreases from 0.336 to 0.504 g; the ΔM_{PGA} area also

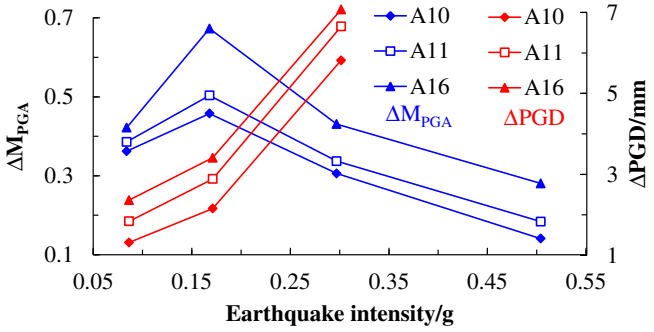

(a) Input in *z*-direction

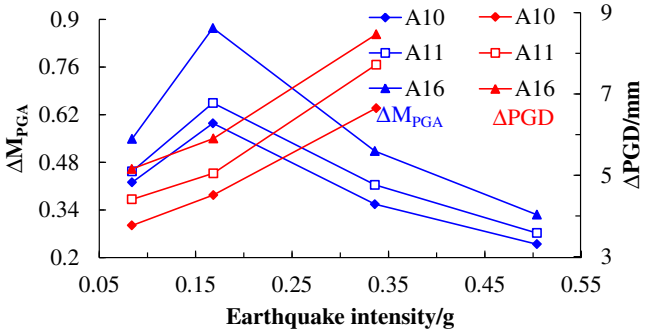

(b) Input in *x*-direction

Fig. 16 Relationship between ΔM_{PGA} and ΔPGD after rapid drawdown for **a** in *z* direction and **b** in *x* direction

decreases and is localized on the platform area. This is because the surface slope has been damaged, and the amplification effect decreases. Therefore, the acceleration amplification effect of the slope increases with increasing seismic loading, but the ΔM_{PGA} decreases from 0.168 to 0.504 g under rapid water drawdown.

Analysis of the damage deformation process

To further clarify the slope damage deformation under the combined action of earthquakes and rapid drawdown, the change in the ΔM_{PGA} and ΔPGD of the three blocks under rapid water drawdown were also analyzed, as shown in Fig. 16. Figure 16 shows that the change in ΔM_{PGA} and ΔPGD is different with increasing earthquake intensity. The ΔM_{PGA} first increases from 0.084 to 0.168 g and then gradually decreases from 0.168 to 0.504 g, but the ΔPGD increases linearly with the increasing earthquake intensity. The influence of rapid drawdown on the slope deformation under the earthquake excitation is clearer in the analysis of the PGD. There is no obvious deformation observed from 0.084 to 0.168 g, indicating that the ΔM_{PGA} increases rapidly, due to the following two reasons. First, water infiltrates into the slope through cracks and softens the joints and slip surface material. Second, the rapid water drawdown promotes the deformation of the slope by producing an unloading effect of the slope and a water hammer effect in the cracks, increasing the inertial force and the downward drag force of the surface slope. Finally, this leads to the gradual decrease in the ΔM_{PGA} after rapid drawdown, and the surface slope transitions from an elastic state to a plastic state when the ΔM_{PGA} is > 0.168 g. However, the surface displacement always increases due to the increasing deformation of the surface slope, which leads to the overall increase in the ΔPGD. Therefore, the M_{PGA} and PGD increase after rapid drawdown, as shown in Fig. 16. Rapid drawdown has less of an influence on the M_{PGA} and a greater impact on the PGD with increasing earthquake intensity. Moreover, a rapid increase in the PGD can be identified under the combined action of earthquakes and rapid drawdown, but the change in the M_{PGA} is not obvious, particularly when the slope damage begins, for example, when the earthquake intensity is > 0.168 g.

Slope damage phenomenon

The dynamic failure process of the slope is shown in Fig. 17. Figure 17a shows that no obvious cracks appear when the seismic intensity is < 0.168 g. Figure 17b shows that the initial rupture follows the crack near the slope surface when the seismic intensity reaches 0.336 g, and many cracks appear between the high and low water levels. The cracks propagate further, deepen, and often connect, but at this stage, the sliding body has not yet formed. Figure 17c shows that more cracks appear in a wider area, and a large deformation can be found on the surface slope when the seismic intensity is 0.504 g. Finally, when the seismic load reaches a threshold value, the surface slope divides into multiple separate blocks, and surface slope slides along the slip surface, which was observed along the gray paperboard, as shown in Figs. 17d and 18. The dynamic failure process can also be divided into three stages based on the deformation phenomenon: the stage with no obvious deformation (< 0.168 g), the stage in which large deformation occurs (0.168–0.336 g), and the stage in which damage occurs (> 0.336 g).

Additionally, Fig. 17d also shows that the settlement and sliding deformation can be observed at the top of the slope, which is because the acceleration amplification effect at the top of the slope is the most intense. Figure 17c, d shows that the area between the high and low water levels is damaged more intensely. Importantly, the rapid water drawdown and water infiltration greatly impact the deformation of the area and promote the deformation of the surface slope. Their influence can be summarized as follows. First, the seepage line of the slope was mainly along the slip surface and cracks along the joints in the surface slope, as shown in Fig. 18. Many cracks occur at the surface slope during the earthquake. Reservoir water infiltrates into the slope through the cracks below the high water level, which reduces the strength of the joints and slip surface materials and allows the cracks to propagate, which reduces the sliding resistance of the slope. Second, the rapid water drawdown creates an unloading effect in the slope and water hammer effect in the cracks as well as increases the inertial force of the surface slope, which further promotes the slope deformation. Third, the rapid water drawdown also increases the sliding force of the surface slope by reducing its sliding resistance, particularly between the high and low water levels. Given the effect of the reservoir water, the infiltration and rapid drawdown promote crack propagation both laterally and vertically, which further weakens the slope and facilitates its

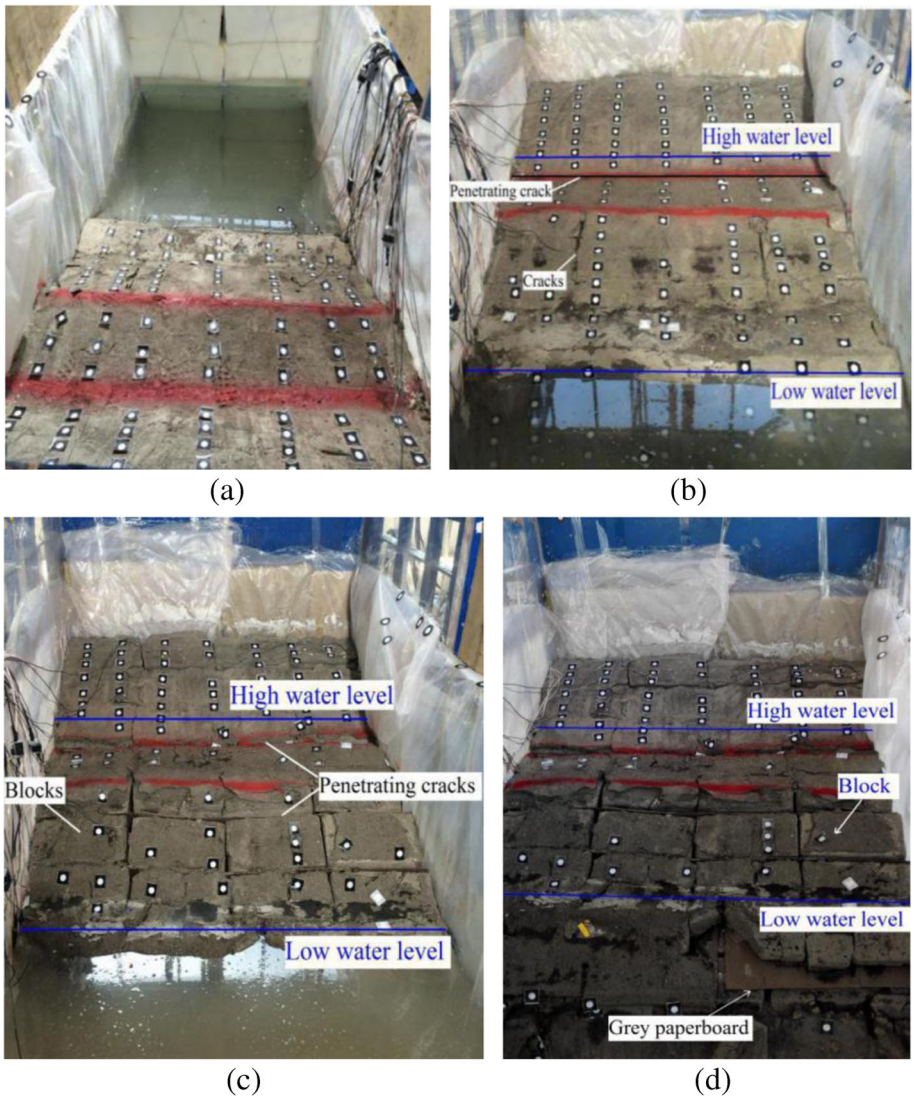

Fig. 17 Failure process of slope model after rapid water drawdown. **a** 0.168 g. **b** 0.336 g. **c** 0.504 g. **d** The final damage phenomenon

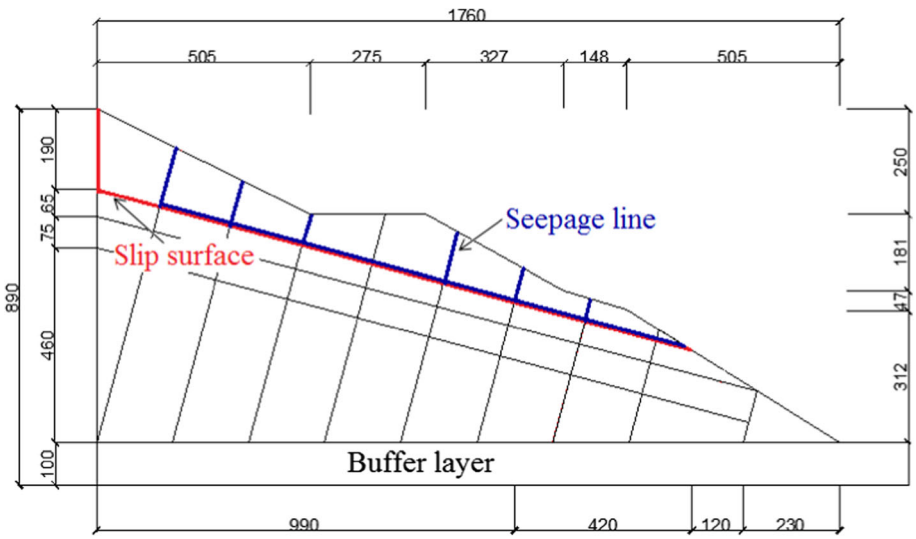

Fig. 18 Deformation characteristics of the slope affected by reservoir water (unit: mm)

deformation. Therefore, under the combined action of earthquakes and reservoir rapid drawdown, the surface slope will undergo block sliding along the first structured plane.

In conclusion, according to the analysis of the dynamic response characteristics of the slope, some problems require more attention during the construction process of the Jinsha River bridge. In terms of the actual engineering design, the anchor and bridge pier positions in the Lijiang bank slope are critical, and their stability should monitored. The bridge pier is in the platform, as shown in Fig. 2b, and its dynamic stability has been affected to a large degree by the earthquakes and rapid drawdown, since the M_{PGA} and PGD of the platform are much larger than the surrounding areas. After the completion of the proposed reservoir, the test results suggest that the reservoir water drawdown speed should be controlled. Moreover, the damage phenomenon of the model slope shows that the platform was damaged seriously when the seismic intensity was > 0.336 g; therefore, the bridge pier should be reinforced to avoid future damage during a large earthquake. In addition, the test results show that the M_{PGA} and PGD near the anchorage are small, indicating that the anchorage is stable during earthquakes, and the current anchorage position is reasonable.

Conclusions

A series of shaking table tests were performed to study the dynamic response characteristics of a rock slope with discontinuous joints under rapid water drawdown. In addition, the XTDIC measurement system was used to analyze the slope surface displacement. The conclusions are as follows:

1. The wave propagation direction greatly impacts the slope deformation. The main deformation style of the slope is settlement and horizontal movement when the seismic wave input is in the z and x directions, respectively. The deformation of the surface slope is larger when the seismic input is in the x direction than the z direction. The PGD under horizontal earthquake loading is approximately 1.3–1.5 times greater than the PGD under vertical earthquake loading, while the M_{PGAx} is approximately 1.2–1.3 times greater than the M_{PGAz}, overall.
2. From the analysis of the ΔPGD and ΔM_{PGA}, the rapid water drawdown has a greater impact on the deformation of the slope surface, particularly between high and low water levels, and the amplification effect is more clearly affected by the S wave. The water infiltration through the cracks softened the material of the surface slope, and the rapid drawdown also enhanced the slope deformation. The deformation process of the slope can be divided into three stages based on the observed test phenomenon: a stage with no obvious deformation (< 0.168 g), a stage in which large deformation occurs (0.168–0.336 g), and a stage in which damage occurs (> 0.336 g). The deformation process of the slope can also be divided into three stages according to the analysis of the PGD and M_{PGA}: an elastic stage (< 0.168 g), a plastic stage (0.168–0.336 g), and a failure stage (> 0.336 g). Additionally, the deformation process of the slope during the earthquake can be identified according to either the M_{PGA} or PGD, but it can be explained more clearly by using the PGD, particularly when the large deformation of the slope first occurs; in this case, the rapid increase in the PGD can reflect the deformation more clearly than the M_{PGA}. The influence of the rapid drawdown on the slope deformation under earthquake excitation is most clearly observed by analyzing the ΔPGD.
3. The settlement deformation and sliding deformation induced by the P waves and S waves, respectively, were the main deformation styles observed in the surface slope. The effects of the wave propagation in the slope under rapid drawdown are as follows. First, the rock mass on the slope shakes vertically due to the P waves, and lateral cracks form on the slope surface, and settlement deformation occurs. Second, a larger horizontal shear deformation of the rock slope is induced by the strong horizontal shaking from the S waves. The differential settlement and horizontal movement of the blocks in the surface slope lead to the formation of many cracks during the earthquake. Third, the water infiltration softens the joints and structural surface, and the rapid water drawdown promotes the slope deformation. Finally, under the combined action of earthquakes and rapid drawdown, the surface slope undergoes block sliding along the slip surface.

Acknowledgments

This work is supported by the National Natural Science Foundation of China (No. 11372180). The authors would like to express their gratitude to Zhijian Wu of Key Laboratory of Loess Earthquake Engineering, CEA, Gansu Province, for their helpful advice.

References

Berilgen MM (2007) Investigation of stability of slopes under water drawdown conditions. Comput Geotech 34(2):81–91. https://doi.org/10.1016/j.compgeo.2006.10.004

Che A, Yang H, Wang B, Ge X (2016) Wave propagations through jointed rock masses and their effects on the stability of slopes. Eng Geol 201:45–56. https://doi.org/10.1016/j.enggeo.2015.12.018

Chen Z, Hu X, Xu Q (2016) Experimental study of motion characteristics of rock slopes with weak intercalation under seismic excitation. J Mt Sci 13(3):546–556. https://doi.org/10.1007/s11629-014-3212-0

Dai F, Xu C, Yao X, Xu L, Tu X, Gong Q (2011) Spatial distribution of landslides triggered by the 2008 Ms 8.0 Wenchuan earthquake, China. J Asian Earth Sci 40(4):883–895. https://doi.org/10.1016/j.jseaes.2010.04.010

Dong H, Gratchev I, Balasubramaniam A (2015) Back analysis of a natural jointed rock slope based on the photogrammetry method. Landslides 12(1):147–154

Fan G, Zhang J, Wu J et al (2016) Dynamic response and dynamic failure mode of a weak intercalated rock slope using a shaking table. Rock Mech Rock Eng 49(8):1–14

Fu X, Sheng Q, Zhang Y, Chen J, Leng X (2016) Extension of the discontinuous deformation analysis method to simulate seismic response of a large rock cavern complex. Int J Geomech 17(5):E4016008

Gao Y, Zhu D, Lei G et al (2014) Stability analysis of three-dimensional slopes under water drawdown conditions. Can Geotech J 51(6):1355–1364. https://doi.org/10.1139/cgj-2013-0448

Gao Y, Yin Y, Li B et al (2017) Characteristics and numerical runout modeling of the heavy rainfall-induced catastrophic landslide–debris flow at Sanxicun, Dujiangyan, China, following the Wenchuan Ms 8.0 earthquake. Landslides 14(4):1–14

Garevski M, Zugic Z, Sesov V (2013) Advanced seismic slope stability analysis. Landslides 10(6):729–736. https://doi.org/10.1007/s10346-012-0360-6

Hong Y, Chen R, Wu C et al 2005. Shaking table tests and stability analysis of steep nailed slopes. Canadian Geotechnical Journal 42(5):1264–1279

Huang R, Li W (2009) Analysis of the geo-hazards triggered by the 12 May 2008 Wenchuan earthquake, China. Bull Eng Geol Environ 68(3):363–371. https://doi.org/10.1007/s10064-009-0207-0

Huang R, Zhao J, Ju N, Li G, Lee ML, Li Y (2013) Analysis of an anti-dip landslide triggered by the 2008 Wenchuan earthquake in China. Nat Hazards 68(2):1021–1039. https://doi.org/10.1007/s11069-013-0671-5

Huang Z, Jiang Z, Zhu S, Wu X, Yang L, Guan Y (2016) Influence of structure and water pressure on the hydraulic conductivity of the rock mass around underground excavations. Eng Geol 202:74–84. https://doi.org/10.1016/j.enggeo.2016.01.003
Jiang T, Liu Y, Ma J (2013) Time history response analysis of jointed rock slope under seismic loads. Chin J Rock Mech Eng 32:3938–3944
Jiang M, Jiang T, Crosta GB, Shi Z, Chen H, Zhang N (2015) Modeling failure of jointed rock slope with two main joint sets using a novel DEM bond contact model. Eng Geol 193:79–96. https://doi.org/10.1016/j.enggeo.2015.04.013
Lin ML, Wang KL (2006) Seismic slope behavior in a large-scale shaking table model test. Eng Geol 86(2):118–133. https://doi.org/10.1016/j.enggeo.2006.02.011
Lin Y, Leng W, Yang G et al (2015) Seismic response of embankment slopes with different reinforcing measures in shaking table tests. Nat Hazards 76(2):791–810. https://doi.org/10.1007/s11069-014-1517-5
Liu H, Xu Q, Li Y (2014a) Effect of lithology and structure on seismic response of steep slope in a shaking table test. J Mt Sci 11(2):371–383. https://doi.org/10.1007/s11629-013-2790-6
Liu Y, Li H, Xiao K, Li J, Xia X, Liu B (2014b) Seismic stability analysis of a layered rock slope. Comput Geotech 55(1):474–481. https://doi.org/10.1016/j.compgeo.2013.10.002
Lu L, Wang ZJ, Song ML, Arai K (2015) Stability analysis of slopes with ground water during earthquakes. Eng Geol 193:288–296. https://doi.org/10.1016/j.enggeo.2015.05.001
Maihemuti B, Wang E, Hudan T et al (2016) Numerical simulation analysis of reservoir bank fractured rock-slope deformation and failure processes. Int J Geomech 16(2):04015053
Massey C, Pasqua FD, Holden C et al (2017) Rock slope response to strong earthquake shaking. Landslides 14(1):249–268. https://doi.org/10.1007/s10346-016-0684-8
Moregenstern N (2015) Stability charts for earth slopes during rapid drawdown. Géotechnique 13(2):121–131
Shinoda M (2015) Seismic stability and displacement analyses of earth slopes using non-circular slip surface. Soils Found 55(2):227–241. https://doi.org/10.1016/j.sandf.2015.02.001
Song Y, Huang D, Cen D (2016) Numerical modeling of the 2008 Wenchuan earthquake-triggered Daguangbao landslide using a velocity and displacement dependent friction law. Eng Geol 215:50–68. https://doi.org/10.1016/j.enggeo.2016.11.003
Toki K, Miura F, Oguni Y (2010) Dynamic slope stability analyses with a non-linear finite element method. Earthq Eng Struct Dyn 13(2):151–171
Wang F, Cheng Q, Highland L, Miyajima M, Wang H, Yan C (2009) Preliminary investigation of some large landslides triggered by the 2008 Wenchuan earthquake, Sichuan Province, China. Landslides 6(1):47–54. https://doi.org/10.1007/s10346-009-0141-z
Wang F, Wang Y, Sun G et al (2011) Study on slope response under seismic loading: taking the Dongshanshiziliang profile in Qingchuan, Sichuan as an example. Geoscience 25(1):142–150
Xia M, Ren G, Ma X (2013) Deformation and mechanism of landslide influenced by the effects of reservoir water and rainfall, Three Gorges, China. Nat Hazards 68(2):467–482. https://doi.org/10.1007/s11069-013-0634-x
Xu B, Yan C (2014) An experimental study of the mechanical behavior of a weak intercalated layer. Rock Mech Rock Eng 47(2):791–798. https://doi.org/10.1007/s00603-013-0420-9
Yang G, Wu F, Dong J et al (2012) Study of dynamic response characters and failure mechanism of rock slope under earthquake. Chin J Rock Mech Eng 31(4):696–702
Zhang S, Zhang L, Glade T (2014) Characteristics of earthquake- and rain-induced landslides near the epicenter of Wenchuan earthquake. Eng Geol 175(11):58–73. https://doi.org/10.1016/j.enggeo.2014.03.012

D. Song · A. Che · R. Zhu · X. Ge
School of Naval Architecture, Ocean and Civil Engineering,
Shanghai Jiao Tong University,
800 Dongchuan-Road, Shanghai, 200040, China

A. Che (✉)
Shanghai, China
Email: alche@sjtu.edu.cn